*Solid State Science and Technology, Vol. 24, No 1(2016) 146-156*
ISSN 0128-7389 | *http://journal.masshp.net*

# EFFECT OF CALCINATION ON STRUCTURAL AND MAGNETIC PROPERTIES OF $CoFe_2O_4$ SYNTHESIZED VIA CO-PRECIPITATION METHOD

Noor Rasyada Ahmad Latiff, Hassan Soleimani, Hasnah Mohd Zaid, Noorhana Yahya and Muhammad Adil

*Department of Fundamental and Applied Sciences, Universiti Teknologi PETRONAS, Bandar Seri Iskandar, 31750 Tronoh, Perak, Malaysia.*

*Corresponding author: syasya.latiff@gmail.com*

## ABSTRACT

Various nanoparticles have been dispersed in carrier fluid to form functional nanofluids that may work on its own or by applying external stimulating field. Magnetically stimulated nanofluid will be influenced by the magnetic properties of the nanoparticles i.e. saturation magnetization that determine the effectiveness of magnetic domain arrangement. Magnetite has been widely studied as an excellent magnetic material for various field applications. Despite having excellent magnetic properties, it is highly susceptible to oxidation and poses limitation to various applications. Therefore, substitution of cobalt in the magnetite lattice is one of the solutions and has shown a remarkable increase in the magnetic and structural properties of cobalt ferrite, $CoFe_2O_4$. It possesses high chemical stability and excellent magnetic properties that is suitable to be dispersed in fluid for magnetic fluid synthesis. $CoFe_2O_4$ nanoparticles were synthesized via co-precipitation method and its properties were compared with $Fe_3O_4$ to study the effect of $Co^{2+}$ cation substitution on the enhancement of structural and magnetic properties of cobalt ferrite. Magnetic properties e.g. saturation magnetization and coercivity were measured using VSM. Irregular shape of particles was observed for all three samples, with crystallite sizes vary from 37.41 to 50.46 nm, calculated at (311) plane. FTIR analysis confirms the formation of ferrite structure by locating the characteristic peak of tetrahedral metal-oxygen bonding around 580 $cm^{-1}$ in both $Fe_3O_4$ and $CoFe_2O_4$. However, the peak could not be identified in the as-precipitated $CoFe_2O_4$ sample, due to the unwanted impurities e.g. Na and Cl ions which the presence was confirmed by EDX analysis. Post calcination at 600 and 800° C shows remarkable improvement in the saturation magnetization, with highest saturation magnetization of 65.40 emu/g achieve at 800 °C. In conclusion, calcination has improved the structural and magnetic properties of $CoFe_2O_4$ by impurities removal and also enhances the crystallinity of the particles.

*Keywords: cobalt ferrite; magnetic nanoparticles; saturation magnetization; calcination temperature*;

*Solid State Science and Technology, Vol. 24, No 1(2016) 146-156*
ISSN 0128-7389 | *http://journal.masshp.net*

## INTRODUCTION

In enhanced oil recovery, viscosity of the displacing fluid is one of the governing factors that determine the success of residual oil mobilization, especially for the case of polymer flooding [1]. Conventional polymers used as displacing fluid are constrained to the reservoir temperature and salinity, as it will suffer chemical and thermal degradation [2]. Magnetic nanofluids subjected to the magnetic field may overcome those problems and retained the desired properties in the harsh environment. Anoop *et al* (2014) has observed that nanofluids exhibit non-Newtonian characteristics at elevated temperatures and pressures. Though viscosity profile is tremendously affected at temperature beyond 100°C, the viscosity of nanofluids and basefluid, increased as the pressure increased [3]. Using cobalt ferrite, Chand *et al* (2013) has found a relationship between magnetization of ferrofluid and the magnetic properties. It can be deduced that particles size distribution and interactions among them are the governing factors which contribute to the magnetoviscous effect in cobalt ferrite, $CoFe_2O_4$ nanofluid. Its viscosity increases with the strength of the magnetic field (from 0 to 0.95 T) due to greater interaction among particles hence giving rise to the flow resistance [4].

Key parameters of controlling the size, morphology and distribution of $CoFe_2O_4$ nanoparticles have been widely studied by employing various synthesis methods and also surface active agents. The magnetic properties of $CoFe_2O_4$ nanoparticles are more complicated than those of the bulk materials and show size dependence [5]. However, it is noteworthy that besides the crystallite size, the magnetic properties of $CoFe_2O_4$ nanoparticles also show much dependence on the synthesis methods and reaction conditions as the preparation route determine the final distribution of the metal ions in spinel structure [6]. Thermal treatment for instance will affect phase homogeneity and site occupancy of cobalt and iron ions between octahedral and tetrahedral sublattices. Many researchers have employed low temperature synthesis methods *e.g.* sol gel and microemulsion. However, a substantial amount of impurities were detected during analysis, suggesting subsequent heat treatment to improve material properties *e.g.* crystallinity, structural and magnetic [7, 8]. With no heat treatment, low saturation magnetization was recorded. There exists an undesirable effect of heat treating the powder particles as it might be responsible for the undesired growth of particles, giving rise to agglomerated and coarse grains [9, 10].

In ferrofluids, each of the particles carries tiny magnets known as magnetic moment. When subjected to magnetic field, each particle containing approximately $10^4$ Bohr magneton will make alignment with the field and will strongly increase magnetization even at weak magnetic field [11]. The observed values of magnetization in terms of Bohr magneton ($\mu_B$) can be calculated using Equation 1:

$$\mu_B = \frac{M \times M_S}{5585} \tag{1}$$

where *M* is the molecular weight of the sample, *Ms* is the saturation magnetization in emu/g.

In this paper, cobalt ferrite nanoparticles of various calcination temperatures have been synthesized via co-precipitation method to study the effect of calcination temperature on the improvement of the structural and magnetic properties of cobalt ferrite.

## METHODOLOGY

*Synthesis of nanoparticles.*
Cobalt ferrite nanoparticles were synthesized via co-precipitation method, by adapting similar method from [12]. Precursor solutions of 0.4 M iron chloride and 0.2 M cobalt chloride were dissolved separately in de-ionized water and then mixed together. Sodium hydroxide of 3.0 M was added to the salt solution dropwise until reaching pH 12. Subsequently, 1 mL of oleic acid was used as the chelating agent. The reaction was performed at 80°C for 2 hours with vigorous stirring. The precipitate prepared was then cooled to room temperature and centrifuged at 3000 rpm to isolate it from the supernatant liquid. Subsequently, the black precipitate was washed with distilled water several times and was then dried for 24 hours. Subsequent calcination of the amorphous sample takes place in argon environment at three different temperatures; 600, 700 and 800°C which were correspondingly labeled as S600, S700 and S800. Magnetite, $Fe_3O_4$ of 98 % purity was purchased from Sigma-Aldrich and serves as benchmark of the properties improvement for comparison purpose.

*Structural and Magnetic Properties Characterization.*
The structural properties of the sintered samples were characterized by X-ray diffractometer (XRD). Magnetic properties were measured using vibrating sample magnetometer (VSM) up to a maximum applied field of 20,000 Oe. FTIR transmission spectra were taken on Perkin Elmer Spectrum BX model Infrared Spectrophotometer from 300 to 3000 $cm^{-1}$. The Raman spectra were excited by the 514.53 nm line of an argon ion laser (Horiba Jobin Yvon) and collected in a backscattering geometry with spectral resolution 6 $cm^{-1}$. Thermal analysis of the as-precipitated sample was conducted using Thermogravimetric Analyzer (TGA) to identify the suitable calcination temperature for impurities removal and densification. The hysteresis and magnetization measurements were performed using vibrating sample magnetometer with a maximum applied field of 15 kOe at room temperature.

## RESULTS AND DISCUSSION

*Structural properties.*
Figure 1 depicts thermal behavior of the as-precipitated $CoFe_2O_4$ sample as it undergoes transformation with temperature. The profile can be divided into four distinct regions; located around 100, 400, 800 and 1000°C. In the first region of the DTA curve, an endothermic reaction with weight loss is shown, mainly due to the vaporization of water in the sample. At about 400°C, a sharp peak can be observed denoting exothermic reaction, which corresponds to the decomposition of non-reactive organic materials. Another peak of exothermic reaction with a small decrease in the sample weight at 801°C corresponds to the fusion of sodium chloride (NaCl), a by-product of reaction of

NaOH with the chloride precursors which present when is not completely removed during washing and filtration [13]. However, this unwanted byproduct can be eliminated by subsequent washing and drying, as per exhibited on ceria nanoparticles [14, 15]. Heat of crystallization was finally found at 980°C, denoted by the presence of the exothermic peak. Hence, the crystallization process of $CoFe_2O_4$ will be completed at temperature beyond 980°C.

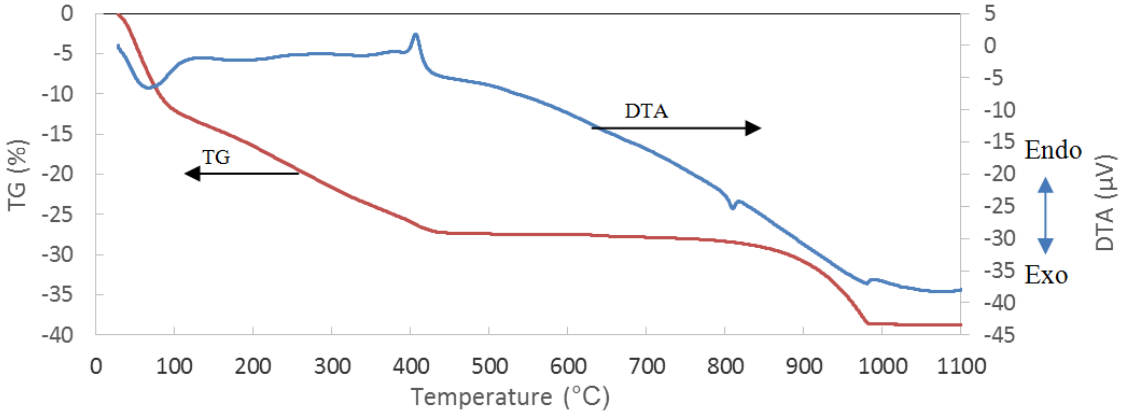


Figure 1: Thermo gravimetric-differential thermal analysis (TG-DTA) curves for as-precipitated $CoFe_2O_4$ samples to find the suitable temperature for annealing

Diffraction patterns for cobalt ferrite samples pre- and post-calcinations shown in Figure 2 were compared with magnetite to study the structural changes imposed by substituting $Fe^{2+}$ with $Co^{2+}$. However, crystallinity of as-precipitated cobalt ferrite was very low and several peaks present (marked with asterisk) could not be indexed to cobalt ferrite which is associated to secondary phase and impurities. From the pattern analysis, the peaks could be partially indexed to NaCl (ICDD 98-002-2521) in agreement to the finding from TG-DTA curves. By calcining the samples from 600 to 800 °C, great changes can be observed in the crystallinity of the samples as narrow peaks of higher intensity appear at all major planes which could be indexed to cobalt ferrite, $CoFe_2O_4$ (ICDD 98-007-9288). The peaks correspond to diffraction planes of typical spinel cubic structure of (111), (220), (311), (400), (422), (511), (440) and (533), respectively [18]. Calcination induces higher and narrower diffraction peaks, indicating increase in crystallinity and also larger crystallite size. Note that the impurities peaks positioned at 31.7, 45.4, 56.4 and 66.2° also begin to diminish as the calcination temperature increases. From the diffraction pattern it is clear that the peaks become sharper with the increase of calcination temperature. This suggests that as the calcination temperature increases the crystallite size also increases [19]. Crystallite size calculation was done using Scherer equation. As calcination temperature changes from 600 to 800 °C, average crystallite size of the sample grows from 37.41 to 50.46 nm. Lattice constant has also expanded from 8.371 to 8.403 Å. By using similar method, Yue Zhang *et. al* (2010) has found expansion in lattice with the increase in particle size [20]. It is also observed that all peaks experience a shift towards lower 2-theta as calcination temperature increases, which indicates higher incorporation

rate of cobalt ions into the lattice as more thermal energy is supplied [21]. This provides a way to distinguish diffraction patterns of various spinel ferrites since the peak shift and lattice constant changes according to the substituted cations. The radius of $Fe^{3+}$ (0.64 Å) is smaller than $Co^{2+}$ (0.72 Å) thus explains the increasing lattice constant as cobalt cation being introduce into the lattice [22]. The variation of the crystallite size and lattice constant at different calcination temperature are shown in Table 1.

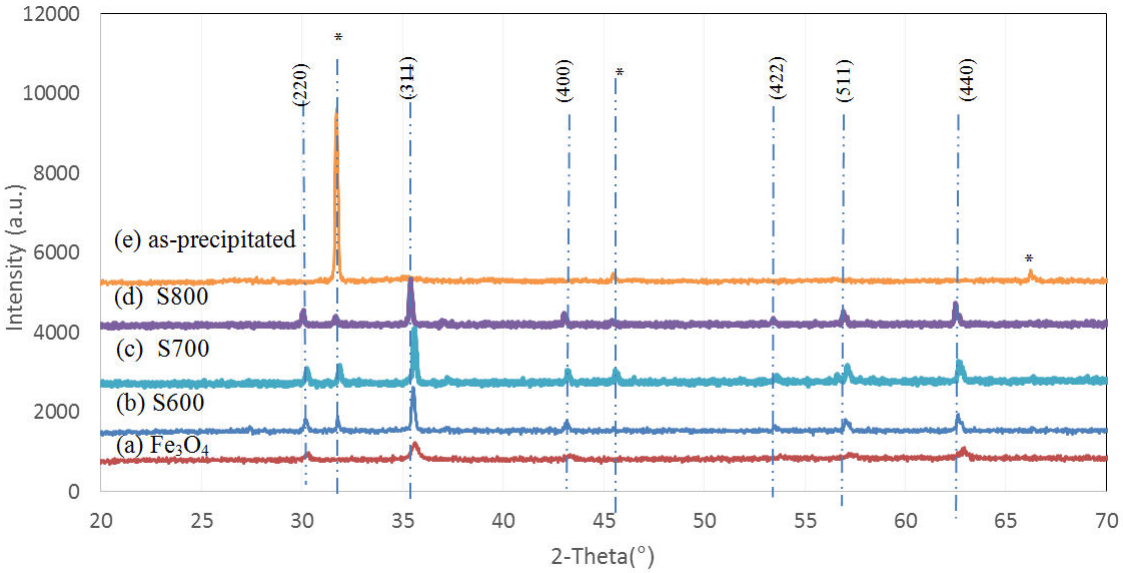


Figure 2: X-ray diffraction patterns for (a) $Fe_3O_4$; $CoFe_2O_4$ (b) sintered at 600°C, (c) sintered at 700°C, (d) sintered at 800°C and (e) as-precipitated. The asterisk mark (*) denotes unwanted peaks associated to NaCl impurities

Table 1: XRD analysis of all samples

| | **Calculated from (311) plane** | | |
|---|---|---|---|
| Sample | Crystallite size [nm] | d-spacing [Å] | Lattice constant [Å] |
| $Fe_3O_4$ | 19.83 | 2.5200 | 8.3580 |
| As-precipitated | 32.05 | 2.5239 | 8.3710 |
| S600 | 37.41 | 2.5239 | 8.3710 |
| S700 | 40.06 | 2.5239 | 8.3710 |
| S800 | 50.46 | 2.5336 | 8.4030 |

FTIR analysis was conducted to investigate the presence of impurities in the material, as well as to identify the bonding between atoms that forms the structure. During synthesis, oleic acid serves as coating agent and its presence can be detected on FTIR spectra at 2924 $cm^{-1}$ and 2854 $cm^{-1}$, for asymmetric $CH_2$ and symmetric $CH_2$ stretch, respectively [23]. As it being chemisorbed on cobalt ferrite surfaces, the peaks shifted to 2922 $cm^{-1}$ and 2849 $cm^{-1}$. For spinel ferrite, the characteristic absorption bands of

interest lies in the range of 350–600 $cm^{-1}$ [24]. The higher frequency absorption band, $\upsilon_1$, is generally observed around 600–500 $cm^{-1}$, which corresponds to intrinsic stretching vibrations of the metal ions at the tetrahedral site. Meanwhile, the lower frequency absorption band, $\upsilon_2$ lies around 350 to 450 $cm^{-1}$ [23, 24]. For our samples, the IR spectra (Figure 3) of cobalt ferrite are found to exhibit two major bands in the range 380–600 $cm^{-1}$ as per listed in Table 2, proving the existence of spinel ferrite [12]. Both $\nu_1$ and $\nu_2$ bands continuously broadened and became less intense with increasing annealing temperature which is commonly observed for inverse spinel ferrites due to the statistical distribution of Fe and Co ions at tetrahedral and octahedral sites [27]. Shifting of both bands toward higher wavenumber as the annealing temperature increases were also observed in this work, which was attributed to the difference in $Fe^{3+}$ – $O^{2-}$ bond length at octahedral and tetrahedral sites [8, 25].

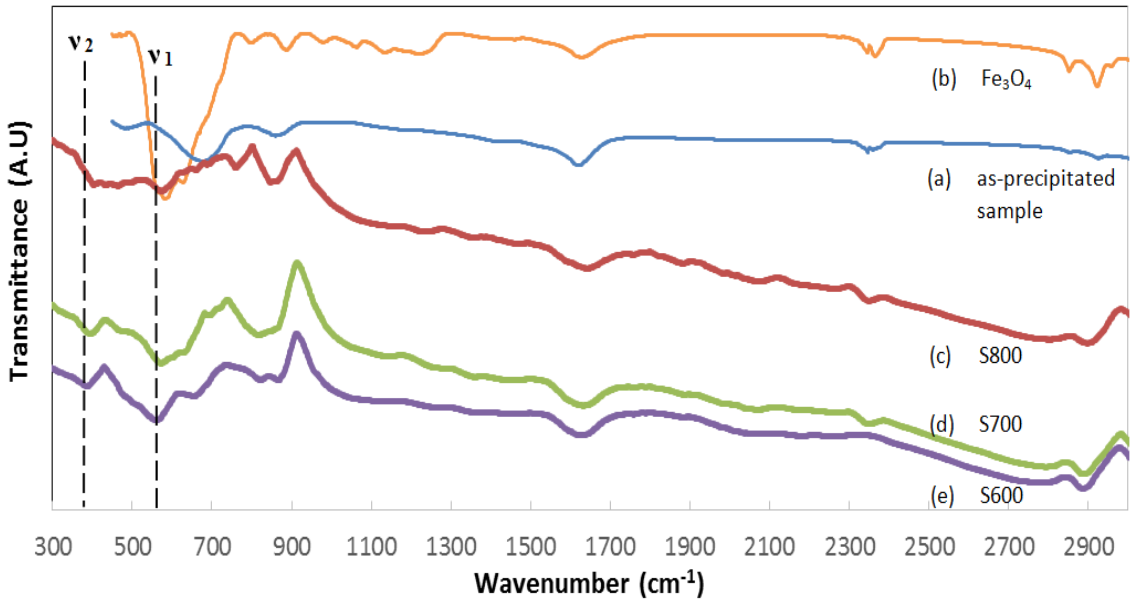


Figure 3: FTIR analysis of cobalt ferrite, $CoFe_2O_4$ nanoparticles (a) $Fe_3O_4$, (b) as-precipitated, (c) annealed at 800°C, (d) annealed at 700°C and (e) annealed at 600°C

Table 2: FTIR analysis of as-precipitated and $CoFe_2O_4$ samples annealed at various temperatures

| | **Wavenumber** | |
|---|---|---|
| Sample | $\nu_1$ ($cm^{-1}$) | $\nu_2$($cm^{-1}$) |
| S600 | 561.04 | 386.08 |
| S700 | 572.05 | 392.81 |
| S800 | 573.67 | 403.00 |
| As-precipitated | 677.19 | - |

Based on the calculation of group theory for $CoFe_2O_4$, there are five allowed Raman active modes ($A_{1g} + E_g + 3F_{2g}$) [26, 27]. For most ferrites, vibrational modes above 600 $cm^{-1}$ considered belong to $A_{1g}$ due to the motion of oxygen in tetrahedral $AO_4$ groups [30]. In Figure 4, A1g mode has appeared at 666 $cm^{-1}$ (S600), 668 $cm^{-1}$ (S700) and 680 $cm^{-1}$ (S800) for the sintered samples. Other bands at lower wavenumbers correspond to the vibrational modes in the octahedral sublattices [6, 28, 29].

*Magnetic Properties.*

The effect of cobalt substitution in magnetite lattice to the enhancement of magnetic properties has been exhibited in the hysteresis loop shown in Figure 5. Magnetic properties *e.g.* saturation magnetization, $M_s$; coercivity, $H_c$ and remanent, $M_r$ are listed in Table 3. The hysteresis loop exhibited ferromagnetic behavior when amorphous phase and impurities present abundantly in as-precipitated sample, and even co-exist after calcination at 600 and 700 °C. At 800 °C, cobalt ferrite sample is approaching paramagnetic behavior as coercivity greatly reduced, almost as low as the coercivity value of magnetite [32]. The as-precipitated sample shows the smallest magnetization (3.01 emu/g) among all samples measured at room temperature which is attributed to the diamagnetic nature of NaCl. The presence of sodium chloride as second phase, as well as other unidentified amorphous phase has been degrading the magnetization of cobalt ferrite samples. Post calcination at 600 °C shows remarkable improvement in the saturation magnetization (36.44 emu/g), as well as the coercivity (149.46 Oe), as wider hysteresis loop can be observed. At 800 °C, highest saturation magnetization (65.40 emu/g) was measured with lowest coercivity among all synthesized samples (81.80 Oe). From XRD analysis, it is observed that higher calcination temperature gives larger crystallite sizes, hence influence the magnetic properties of the samples. Furthermore, partial removal of impurities gives rise to the improvement in magnetic properties. Saturation magnetization of $CoFe_2O_4$ samples was increased from 36.44 to 65.40 emu/g by increasing calcination temperature from 600 to 800 °C (Figure 6). It is significantly lower than that of bulk $CoFe_2O_4$ (73 emu/g), which may be attributed to the distortion of magnetic moments at nanosize particles [28]. It is worth concluding that larger saturation value will be obtained if the sample is being washed and calcined at temperature higher than 800 °C as complete crystallization of $CoFe_2O_4$ occurs at 980 °C [33].

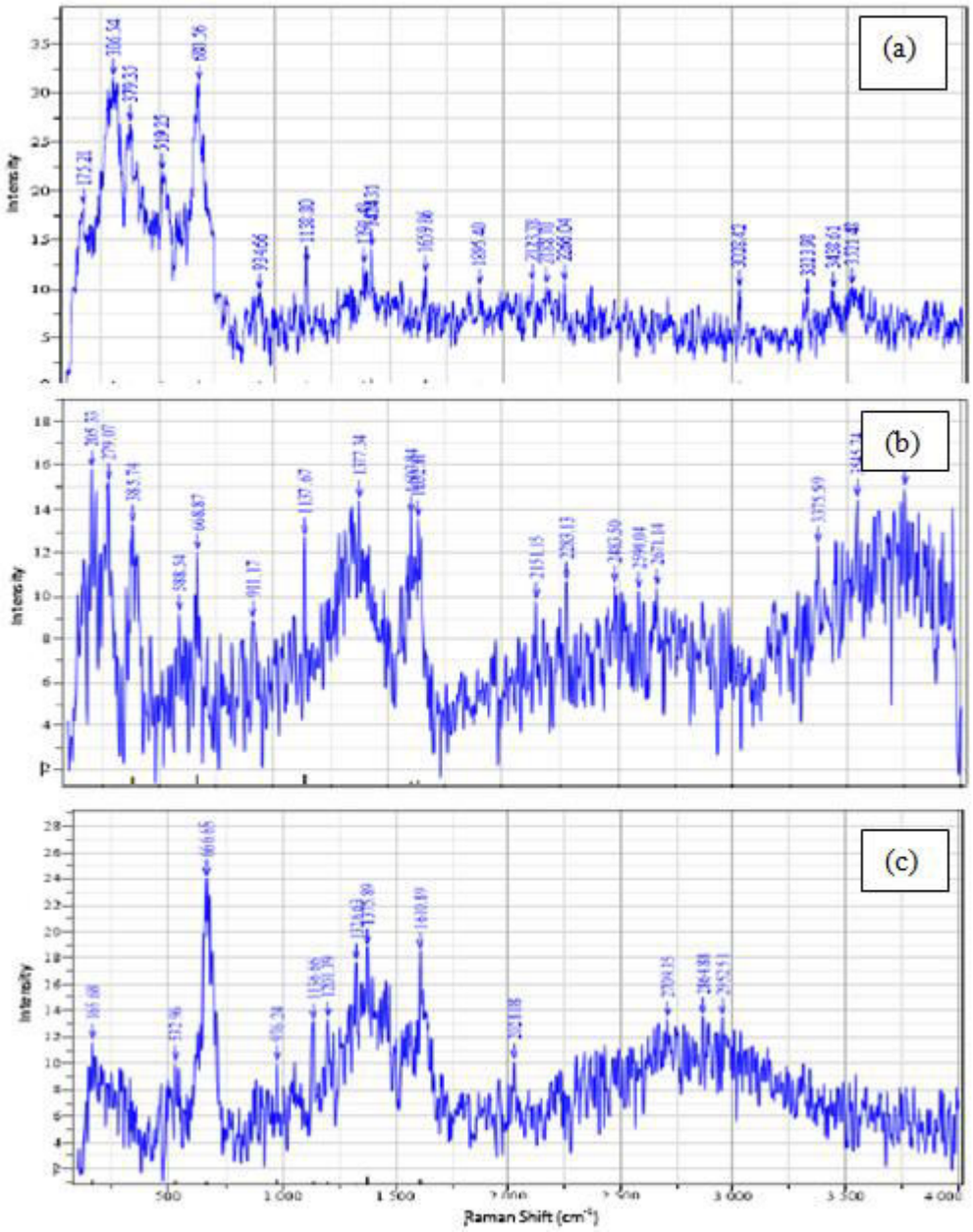


Figure 4: Raman spectra of cobalt ferrite, $CoFe_2O_4$ nanoparticles (a) S800 (b) S700 and (c) S600

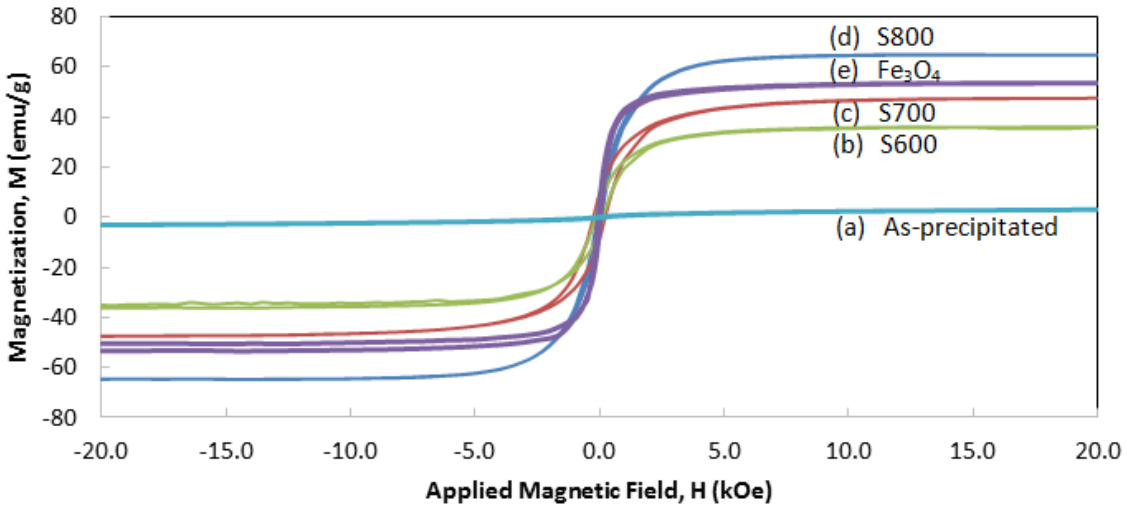


Figure 5: The magnetic hysteresis loops of cobalt ferrite samples; (a) as-precipitated and after calcination at (b) 600, (c) 700, (d) 800 and (e) $Fe_3O_4$

Table 3: Magnetic properties of $Fe_3O_4$ and $CoFe_2O_4$

| **Magnetic Properties** | **S600** | **S700** | **S800** |
|---|---|---|---|
| **Coercivity (Oe)** | 149.46 | 235.57 | 81.80 |
| **Saturation Magnetization (emu/g)** | 36.44 | 47.71 | 65.40 |
| **Remanence (emu/g)** | 5.04 | 9.07 | 5.12 |

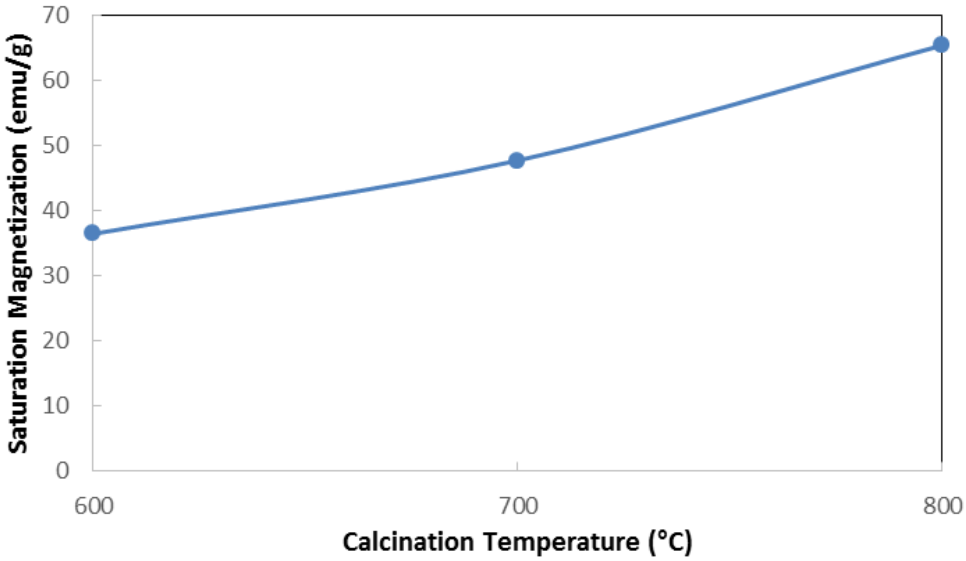


Figure 6: Variation of saturation magnetization value as a function of calcination temperature

## CONCLUSION

Cobalt ferrite nanoparticles have been successfully synthesized via co-precipitation method followed by subsequent calcination in argon environment. Pre-calcination analyses on the samples indicate poor crystallinity with the presence of impurity. Post calcinations at 600 to 800 °C show remarkable improvement in the structural and magnetic properties of $CoFe_2O_4$. From XRD analysis, improved crystallinity was observed with increase in the crystallite size as calcination temperature goes up. Lattice constant has also increases with temperature as more thermal energy is supplied to promote $Co^{2+}$ incorporation in the lattice by substituting $Fe^{2+}$. Larger crystallite size associates with higher saturation magnetization and lower coercivity, hence post calcination at 800°C gives largest particle size (50.46 nm) and highest saturation magnetization (65.40 emu/g). Improvement in *saturation magnetization value* of cobalt ferrite with respect to magnetite is desirable for our future application of ferrofluid in enhanced oil recovery. Magnetic materials dispersed in ferrofluid with high saturation magnetization will have higher viscosity when magnetic field is applied due to the formation of longer chain-like structure which results in flow resistance .

## ACKNOWLEDGMENT

The authors would like to thank the Ministry of Education Malaysia for providing funds; Fundamental Research Grant Scheme (FRGS 0153AB-I46) and MyPhD.

## REFERENCES

[1]. S. K. Veerabhadrappa, T. Urbissinova, J. J. Trivedi, and E. Kuru, "Polymer Screening Criteria for EOR Application - A Rheological Characterization Approach," *SPE West. North Am. Reg. Meet.*, Apr. 2013.

[2]. B. Choi, M. S. Jeong, and K. S. Lee, *Polym. Degrad. Stab.*, **110** 225–231 (2014)

[3]. K. Anoop, R. Sadr, M. Al-Jubouri, and M. Amani, *Int. J. Therm. Sci.*, **77**, 108–115 (2014)

[4]. M. Chand, S. Kumar, A. Shankar, R. Porwal, and R. P. Pant, *J. Non. Cryst. Solids*, **361**38–42 (2013)

[5]. Y. Zhang, Z. Yang, D. Yin, Y. Liu, C. Fei, R. Xiong, J. Shi, and G. Yan, *J. Magn. Magn. Mater.*, **322 (**21) 3470–3475 (2010)

[6]. P. P. C. Sartoratto, M. A G. Soler, T. M. Lima, F. L. R. Silva, T. V. Trufini, V. K. Garg, a. C. Oliveira, and P. C. Morals, *Phys. Procedia*, **9** 10–14 (2010)

[7]. G. A. El-Shobaky, A. M. Turky, N. Y. Mostafa, and S. K. Mohamed, *J. Alloys Compd.*, **493** (3) 415–422 (2010)

[8]. M. S. Khandekar, R. C. Kambale, J. Y. Patil, Y. D. Kolekar, and S. S. Suryavanshi, *J. Alloys Compd.*, (509) 1861–1865 (2011)

[9]. S. C. Goh, C. H. Chia, S. Zakaria, M. Yusoff, C. Y. Haw, S. Ahmadi, N. M. Huang, and H. N. Lim, *Mater. Chem. Phys.*, **120** (1) 31–35 (2010)

[10]. K. Maaz, A. Mumtaz, S. K. Hasanain, and A. Ceylan, *J. Magn. Magn. Mater.*, **308** 289–295 (2007)

[11]. S. Odenbach, *Colloids Surfaces A Physicochem. Eng. Asp.*, **217** (1–3) (171–178) (2003)
[12]. M. H. Habibi and H. J. Parhizkar, *Spectrochim. Acta - Part A Mol. Biomol. Spectrosc.*, **127** 102–106 (2014)
[13]. P. Yang, D. Wang, J. Zhao, and R. Shi, *Mater. Res. Bull.*, **65** 36–41 (2015)
[14]. Y. X. Li, W. F. Chen, X. Z. Zhou, Z. Y. Gu, and C. M. Chen, *Mater. Lett.*, **59** (1) 48–52 (2005)
[15]. D. Sergeev, D. Kobertz, and M. Müller, *Thermochim. Acta*, **606** 25–33 (2015)
[16]. M. Khalid, M. Mujahid, S. Amin, R. S. Rawat, a. Nusair, and G. R. Deen, *Ceram. Int.*, **39** (1) 39–50 (2013)
[17]. C. V. Reddy, S. V. PrabhakarVattikuti, R. V. S. S. N. Ravikumar, S. J. Moon, and J. Shim, *J. Magn. Magn. Mater.*, **394** 70–76 (2015)
[18]. R. Rani, S. K. Sharma, K. R. Pirota, M. Knobel, S. Thakur, and M. Singh, *Ceram. Int.*, **38** (3) 2389–2394 (2012)
[19]. H. Kumar, R. C. Srivastava, P. Negi, H. M. Agrawal, and A. Singh, *Int. J. Mater. Eng. Innov.*, **5** (3) 227 (2014)
[20]. Y. Zhang, Z. Yang, D. Yin, Y. Liu, C. Fei, R. Xiong, J. Shi, and G. Yan, *J. Magn. Magn. Mater.*, **322** 3470–3475 (2010)
[21]. L. Kumar and M. Kar, *Ceram. Int.*, **38** 4771–4782 (2012)
[22]. N. T. Lan, N. P. Duong, and T. D. Hien, *J. Alloys Compd.*, **509** 5919–5925 (2011)
[23]. L. Zhang, R. He, and H. C. Gu, *Appl. Surf. Sci.*, **253**, (5) 2611–2617 (2006)
[24]. R. Sa, A. Ghasemi, R. Shoja-razavi, and M. Tavousi, *J. Magn. Magn. Mater.*, **396** 288–294 (2015)
[25]. Q. Ba, C. Ban, H. Zeng, and G. Zeng, *Science (80)*, **239** 495–497 2002
[26]. L. Kumar, P. Kumar, and M. Kar, *J. Alloys Compd.*, **551** 72–81 (2013)
[27]. L. Kumar, P. Kumar, A. Narayan, and M. Kar, *Int. Nano Lett.*, **3** (1) 8 (2013)
[28]. Y. Qu, H. Yang, N. Yang, Y. Fan, H. Zhu, and G. Zou, *Mater. Lett.*, 60 3548–3552 (2006)
[29]. R. Bujakiewicz-Korońska, Ł. Hetmańczyk, B. Garbarz-Glos, A. Budziak, A. Kalvane, K. Bormanis, and K. Drużbicki, *Cent. Eur. J. Phys.*, **10** (5) 1137–1143 (2012)
[30]. Z. Wang, D. Schiferl, Y. Zhao, and H. S. C. O'Neill, *J. Phys. Chem. Solids*, **64** (12) 2517–2523 (2003)
[31]. T. Yu, Z. X. Shen, Y. Shi, and J. Ding, *J. Phys. Condens. Matter*, **14** (37), L613–L618 (2002)
[32]. S. Ayyappan, G. Panneerselvam, M. P. Antony, and J. Philip, *Mater. Chem. Phys.*, **130** (3) 1300–1306 (2011)
[33]. M. Sajjia, M. Oubaha, T. Prescott, and A. G. Olabi, *J. Alloys Compd.*, **506** 400–406 (2010)